Theoretical Study on the Nonadiabatic Transitions in the Photodissociation of Cl_2, Br_2, and I_2

Yukako Asano† and Satoshi Yabushita*

Department of Chemistry, Faculty of Science and Technology, Keio University, 3-14-1 Hiyoshi, Kohoku-ku, Yokohama 223-8522, Japan
Received March 4, 2003

We have theoretically studied the nonadiabatic transitions among the five lower states with the $\Omega=1_u$ symmetry ($1_u^{(1)}$ to $1_u^{(5)}$) in the photodissociation of Cl_2, Br_2, and I_2 by using the spin-orbit configuration interaction (SOCI) method and the semiclassical time-dependent coupled Schrödinger equations. From the configuration analyses of the SOCI wavefunctions, we found that the nonadiabatic transition between $1_u^{(2)}$ and $1_u^{(1)}$ is a noncrossing type, while that between $1_u^{(3)}$ and $1_u^{(4)}$ is a crossing type for all the molecules. The behavior of the radial derivative coupling element between $1_u^{(1)}$ and $1_u^{(2)}$ and that between $1_u^{(3)}$ and $1_u^{(4)}$ is analyzed in detail. In Cl_2, nonadiabatic transitions can take place even between the states correlating to different dissociation limits, while in Br_2 and I_2, with the usual photon energies e.g. less than 20 eV, nonadiabatic transitions occur only between the states correlating to the same dissociation limits, reflecting the different magnitudes of the spin-orbit interactions.

Key Words : Photodissociation, Nonadiabatic transition, Spin-orbit interaction, SOCI method, Noncrossing-type transition

Introduction

Diatomic halogen and interhalogen molecules continue to serve as benchmark systems to study photodissociation dynamics, with a special interest in relatively large variations in the spin-orbit (SO) interactions, for example, the SO splitting of Cl, Br, and I is 881, 3685, and 7603 cm^{-1}, respectively. Recent experimental activity has been devoted to the study of the orientation and alignment, namely the m_J distributions, of the product angular momentum. Details of the nonadiabatic transition probabilities have been estimated from such analyses for Cl_2[1-4] and Br_2.[3]

We distinguish in this paper the SO states $X(^2P_{3/2})$ and $X(^2P_{1/2})$ of a halogen atom as X and X*, respectively, and label the five $\Omega = 1_u$ states of a halogen molecule X_2 in the energetic order as $1_u^{(1)}$ through $1_u^{(5)}$. Our theoretical potential curves[5,6] of the relevant states of Cl_2 and Br_2 are shown in Figure 1 and those of I_2 in Figure 2. Note the similarities and differences in their potential curves.

In a previous paper,[6] we evaluated the nonadiabatic transition probabilities of Cl_2 and Br_2 by solving the semiclassical time-dependent coupled Schrödinger equations. The nonadiabatic transition from $1_u^{(2)}$ to $1_u^{(1)}$ is of non-crossing type and the heavier Br_2 behaves more adiabatically than Cl_2, as experimentally observed by Kitsopoulos *et al.*[3] Recent experimental works[1-4] have suggested significant photon energy dependence of this nonadiabatic transition probability in Cl_2, which attracts a theoretical interest. By contrast, the nonadiabatic transition from $1_u^{(3)}$ to $1_u^{(4)}$ is found as a crossing type and Cl_2 behaves more adiabatically than Br_2.[6] Since these two nonadiabatic transitions show a completely opposite trend, it is interesting to analyze further the corresponding nonadiabatic transitions in I_2.

Balasubramanian *et al.*[7] calculated the spectroscopic properties and potential curves of I_2 by the complete active space SCF method followed by the first-order and second-order configuration interaction (CI), and relativistic CI methods. Teichteil and Pelissier[8] calculated the potential curves of I_2 with an *ab initio* relativistic atomic pseudo-potential method and analyzed the available experimental data. Nieuwpoort *et al.*[9] employed an all-electron Dirac-Fock method followed by the CCSD(T) calculations. However, none of the previous workers has studied the nonadiabatic transitions in the photodissociation of I_2.

In this paper, we calculate the potential curves of I_2 by the spin-orbit configuration interaction (SOCI) method, and evaluate the radial derivative coupling elements among the five lower states with the $\Omega=1_u$ symmetry ($1_u^{(1)}$ to $1_u^{(5)}$) to examine the nonadiabatic transition processes and to compare the results with those of Cl_2 and Br_2.[5,6] It will be clear that the SO interactions play a very crucial role in the behavior of these nonadiabatic transitions.

Computational Methods

We used the RECPs by Christiansen *et al.*[10] with the 5s5p valence shell for I. The associated valence basis functions of (3s,3p) were used without contraction and augmented by a set of diffuse s and p (α_s = 0.0381, α_p = 0.04664) functions. We added two sets of spherical d-polarization functions (α_d = 0.3724 and 0.19) and a set of spherical f-polarization

*Corresponding Author: Fax: +81-45-566-1697, E-mail: yabusita@chem.keio.ac.jp
†Present address: Mechanical Engineering Research Laboratory, Hitachi, LTD. 502 Kandatsu, Tsuchiura 300-0013, Japan

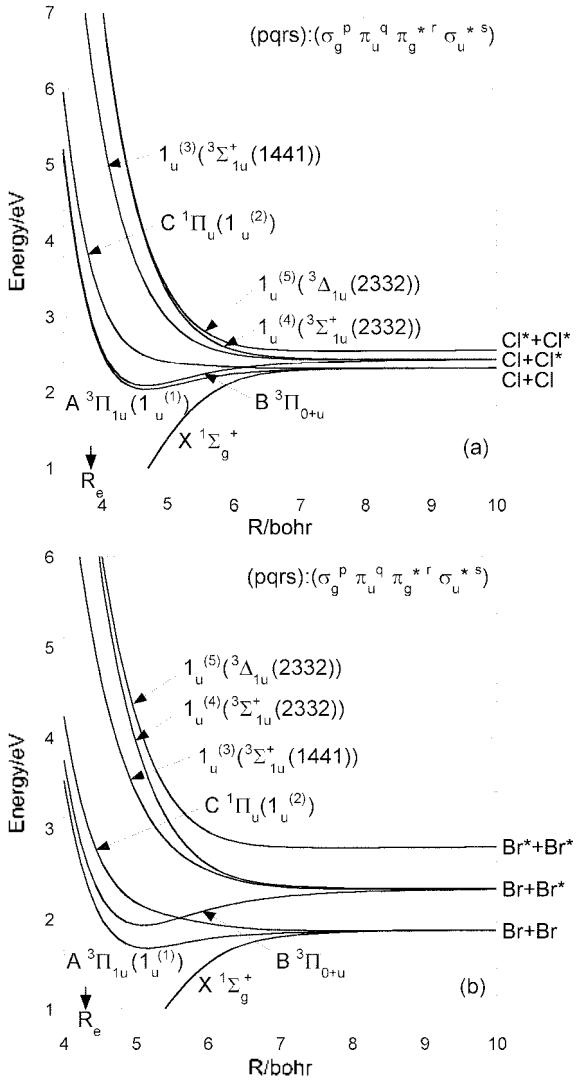

Figure 1. (a) Adiabatic potential curves of Cl_2 obtained from the contracted spin-orbit CI calculation. Numbers (*pqrs*) denote the dominant electronic configuration ($\sigma_g^p \pi_u^q \pi_g^{*r} \sigma_u^{*s}$) in the Franck-Condon region. (b) Those of Br_2.

functions ($\alpha_f = 0.3$) and g-polarization functions ($\alpha_g = 0.415$). The basis sets are thus expressed as (4s,4p,2d,1f,1g).

One-electron orbitals for the SOCI calculations must be chosen with a special care to ensure the correct behavior of the potential curves at longer internuclear distances R. We have employed the state-averaged SCF method, in which the molecular orbitals are optimized for the averaged state of all the configurations derived from (σ_g,π_u,π_g*,σ_u*)[10], namely 10 electrons in the six orbitals. Here, σ_g, π_u, π_g*, and σ_u* are the molecular orbitals derived mostly from the 5p atomic orbitals of I.

For the SOCI calculations, singlet and triplet configuration state functions (CSF's) were generated with the reference of (σ_g,π_u,π_g*,σ_u*)[10]. All the single and double excitations from these reference CSF's were included in the second-order CI scheme. We carried out the "contracted SOCI" method where the total Hamiltonian including the SO part was

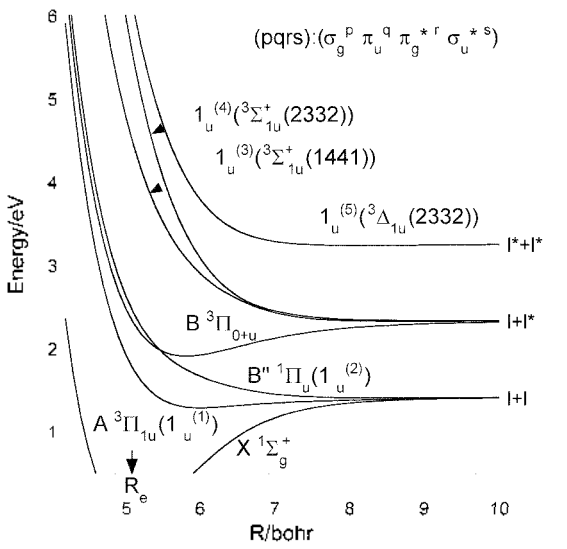

Figure 2. Adiabatic potential curves of I_2 obtained from the contracted spin-orbit CI calculation.

Table 1. Calculated and experimental spectroscopic constants[16,17] for the X $^1\Sigma_g^-$, A $^3\Pi_{1u}$, and B $^3\Pi_{0+u}$ states of Br_2

		R_e (bohr)	D_e (eV)	ω_e (cm^{-1})	$\omega_e x_e$ (cm^{-1})
X $^1\Sigma_g^-$	This work	4.340	1.881	319.9	1.10
	Experiment	4.310	1.971	325.3	1.08
A $^3\Pi_{1u}$	This work	5.153	0.2077	142.3	2.76
	Experiment	5.083	0.2568	153	2.7
B $^3\Pi_{0-u}$	This work	5.098	0.4131	160.2	1.88
	Experiment	5.060	0.4660	167.6	1.64

Table 2. Calculated and experimental spectroscopic constants[16,17] for the X $^1\Sigma_g^-$, A $^3\Pi_{1u}$, and B $^3\Pi_{0+u}$ states of I_2

		R_e (bohr)	D_e (eV)	ω_e (cm^{-1})	$\omega_e x_e$ (cm^{-1})
X $^1\Sigma_g^-$	This work	5.099	1.431	208.9	0.57
	Experiment	5.038	1.543	214.5	0.61
A $^3\Pi_{1u}$	This work	6.002	0.1415	80.44	2.02
	Experiment	5.885	0.2033	92.9	1.57
B $^3\Pi_{0-u}$	This work	5.815	0.4386	115.5	0.90
	Experiment	5.715	0.5304	125.7	0.76

diagonalized in the basis of the 16 "spin-free" (SF) CI eigenstates of 3 × $^1\Sigma_g^-$, $^1\Pi_{ux}$, $^1\Pi_{gx}$, $^1\Sigma_u^-$, $^1\Delta_g$, 3 × $^3\Sigma_u^-$, $^3\Pi_{ux}$, $^3\Pi_{gx}$, $^3\Pi_{uy}$, $^3\Pi_{gy}$, $^3\Sigma_g^-$, and $^3\Delta_u$, all of which correlate with the atomic dissociation limits of I(^{2}P) + I(^{2}P). Here, SF stands for the calculations without the SO interactions. The accuracy of this contracted SOCI method for various iodine containing molecules has been assessed before,[11,12] and an error due to the contraction was found to be at most 0.03 eV in excitation energies. The Davidson correction was included in the CI energy. For Cl_2 and Br_2, we used the results reported in our previous works.[2,5,6] All the SOCI calculations were performed with the COLUMBUS program package[13] with the spin-dependent GUGA.[14,15]

Results and Discussion

Spectroscopic constants and potential curves of Br_2 and I_2. The calculated potential curves of I_2 are shown in Figure 2. Spectroscopic constants of the $X\ ^1\Sigma_g^+$, $A\ ^3\Pi_{1u}$, and $B\ ^3\Pi_{0+u}$ states of Br_2 and I_2 are shown in Table 1 and Table 2, respectively, and are in reasonable agreement with the experimental results.[16,17]

In Figure 2, $1_u^{(3)}$ and $1_u^{(4)}$ for I_2 exhibit an avoided crossing at around $R = 6.6$ bohr. This is due to the configuration switching between the dominant $^3\Sigma_{1u}^-$ (1441) and $^3\Sigma_{1u}^+$ (2332) configurations, where (*pqrs*) stands for the electronic configuration of $\sigma_g^p\pi_u^q\pi_g^{*r}\sigma_u^{*s}$. The corresponding configuration switching takes place also in Cl_2 and Br_2, though their avoided crossing behavior is invisible in Figure 1, and that in Cl_2 was overlooked inadvertently and treated as a non-crossing type in a previous work.[2] This avoided crossing persists in the absence of the SO interactions and will play an important role in the nonadiabatic transition from $1_u^{(3)}$ to $1_u^{(4)}$, as discussed later.

In the Franck-Condon (FC) region of I_2, $1_u^{(4)}$ has the dominant configuration of $^3\Sigma_{1u}^+$ (2332) and $1_u^{(5)}$ has the one of $^3\Delta_{1u}$ (2332) as shown in Figure 2. The same feature was observed for Br_2.[6] On the other hand, for Cl_2, $1_u^{(4)}$ is dominated by $^3\Delta_{1u}$ (2332) and $1_u^{(5)}$ is by $^3\Sigma_{1u}^-$ (2332),[2,5] and these dominant configurations were exchanged at around $R = 3.84$ bohr just outside the equilibrium distance $R_e = 3.811$ bohr,[2,5] as discussed in the next section.

Behavior of electronic wavefunctions and the radial derivative coupling elements. In the contracted SOCI method, the electronic wavefunction for $1_u^{(m)}$ is expanded in terms of the five SFCI eigenstates, namely, $^3\Pi_u(2431)$, $^1\Pi_u(2431)$, $^3\Sigma_u^+(1441)$, $^3\Sigma_u^+(2332)$, and $^3\Delta_u(2332)$ in the FC region, as follows:

$$|1_u^{(m)}\rangle = \sum_{i=1}^{5} \alpha_{i,m} |^{2S_i+1}\Lambda_i\rangle \qquad (1)$$

where $\alpha_{i,m}$ are the R-dependent expansion coefficients obtained by diagonalizing the total Hamiltonian including the SO part in the subspace of the above five SF states $|^{2S_i+1}\Lambda_i\rangle$. For each state $1_u^{(m)}$, the symbol $^{2S_i+1}\Lambda_i$ with the

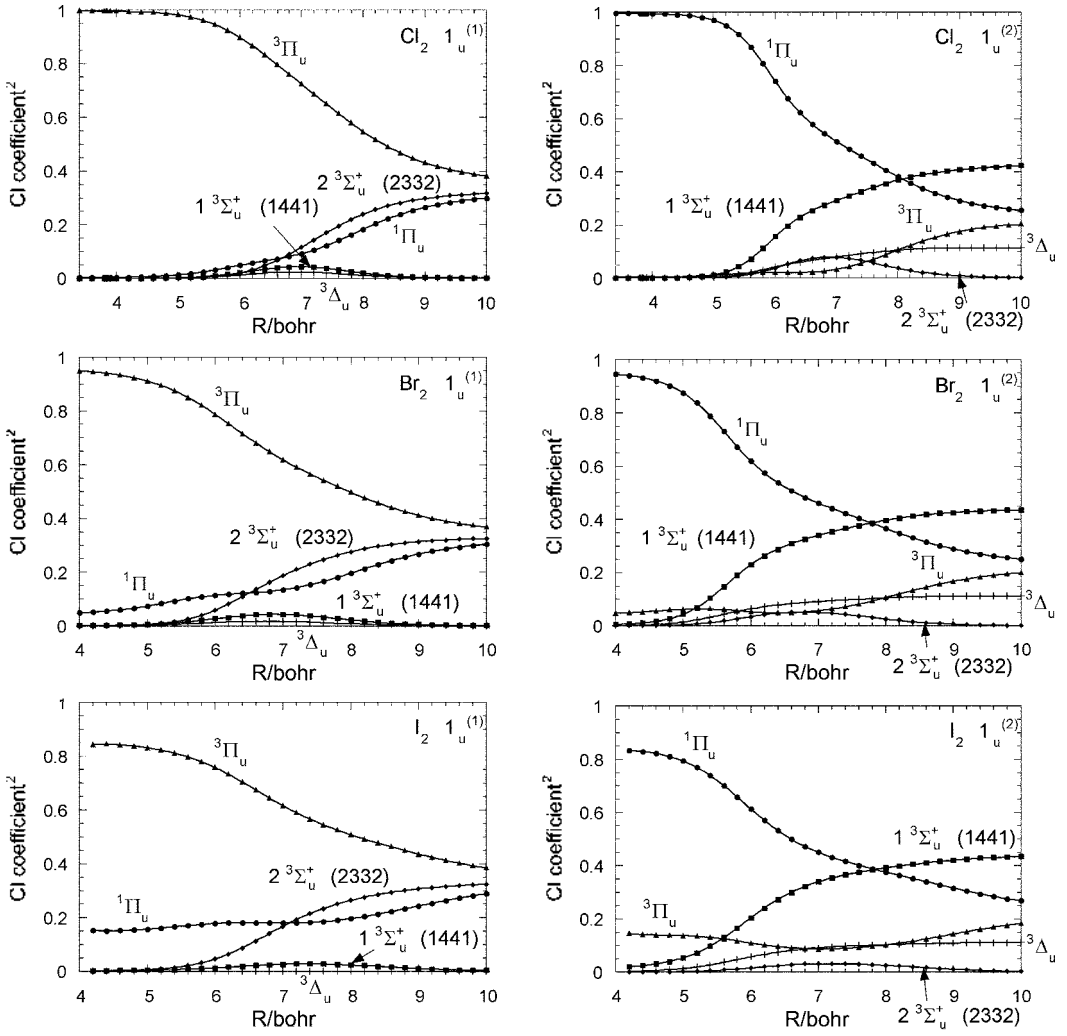

Figure 3. Variations of the weights of the five *LS* configurations to expand the adiabatic states $1_u^{(1)}$ and $1_u^{(2)}$. The upper is for Cl_2, the middle is for Br_2, and the bottom is for I_2.

dominant $\alpha_{i,m}$ value in the FC region is used as the state label in Figures 1 and 2.

The radial derivative coupling elements g_{mn} can be calculated directly with the CI vectors in the contracted SOCI calculation as follows:

$$g_{mn} = \langle 1_u^{(m)} \left| \frac{d}{dR} \right| 1_u^{(n)} \rangle \approx \sum_k c_{k,m}(R) \frac{c_{k,n}(R + \Delta R) - c_{k,n}(R)}{\Delta R} \tag{2}$$

where $c_{k,m}$ is the kth element in the mth CI vector in the CSF basis. The step size ΔR in the numerical differentiation was 4.0×10^{-4} bohr as before.[5] The so-called molecular orbital derivative term was neglected because its contribution is usually small and to the extent of 10-15% at most.[18] This approximation is especially good in this study because the active molecular orbitals σ_g, π_u, π_g*, and σ_u* belong to distinct symmetries and they are derived mostly from 5p atomic orbitals and hardly change at important longer R. Substituting Eq. (1) into Eq. (2), we have.

$$\begin{aligned} g_{mn} &= \sum_{i,j=1}^{5} \alpha_{i,m} \frac{d\alpha_{j,n}}{dR} \langle {}^{2S_i+1}\Lambda_i \left| {}^{2S_j-1}\Lambda_j \right\rangle \\ &+ \sum_{i,j=1}^{5} \alpha_{i,m}\alpha_{j,n} \langle {}^{2S_i+1}\Lambda_i \left| \frac{d}{dR} \right| {}^{2S_j-1}\Lambda_j \rangle \\ &= \sum_{i=1}^{5} \alpha_{i,m} \frac{d\alpha_{i,n}}{dR} + \sum_{i,j=1}^{5} \alpha_{i,m}\alpha_{j,n} \langle {}^{2S_i+1}\Lambda_i \left| \frac{d}{dR} \right| {}^{2S_j+1}\Lambda_j \rangle \end{aligned} \tag{3}$$

The second term in Eq. (3) has no contribution unless $S_i = S_j$, $\Lambda_i = \Lambda_j$, and $i \neq j$ (the last condition comes from the anti-symmetric nature of the derivative coupling elements) and therefore has a contribution only from $\langle 1\text{st } {}^3\Sigma_u^+ | d/dR | 2\text{nd } {}^3\Sigma_u^+ \rangle$. This matrix element has a non-negligible contribution, since even in the SFCI problem, the first and second ${}^3\Sigma_u^-$ SFCI eigenstates exhibit an avoided crossing at a longer R, where the significant configuration mixings take place between the ${}^3\Sigma_u^-$ (1441) and ${}^3\Sigma_u^-$ (2332) configurations, as follows:

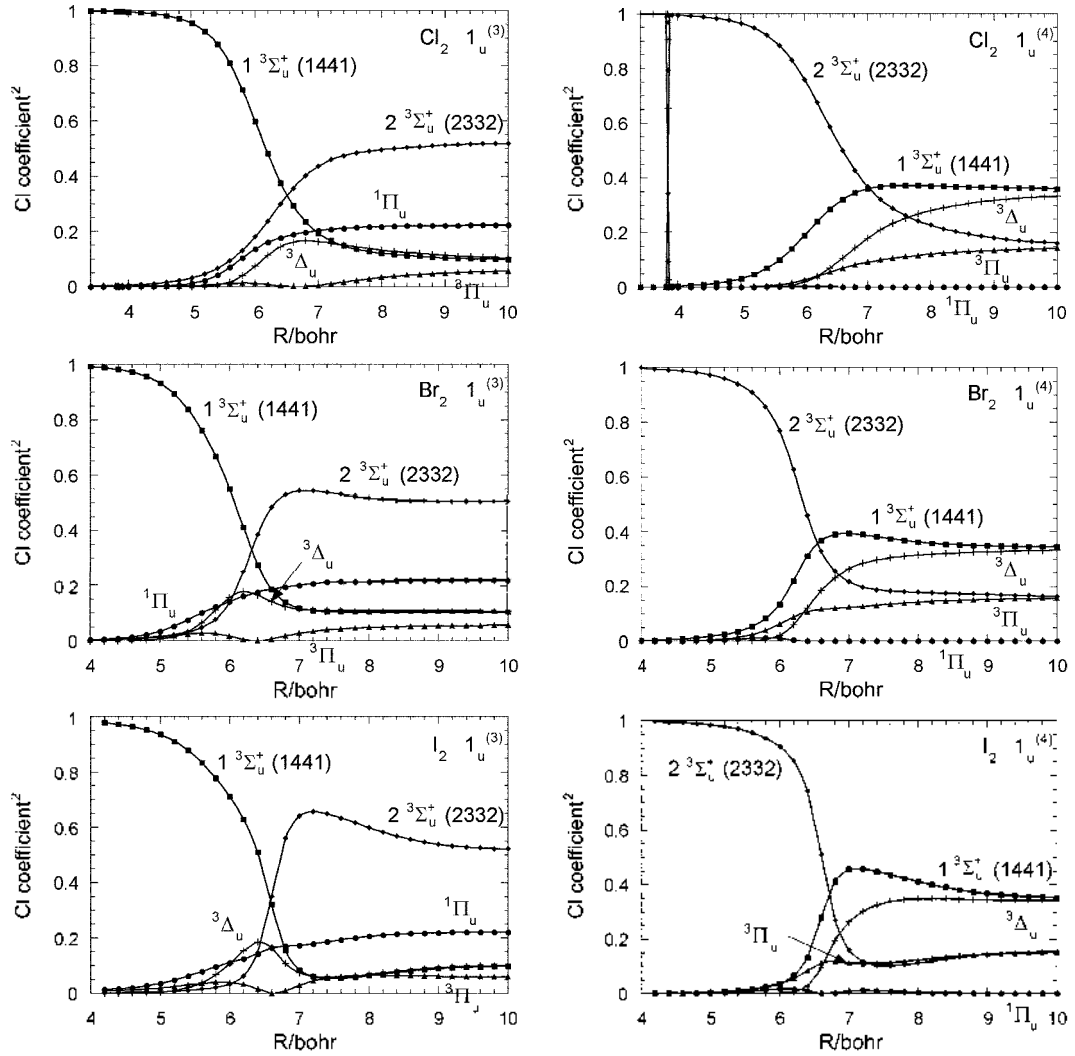

Figure 4. Variations of the weights of the five *LS* configurations to expand the adiabatic states $1_u^{(3)}$ and $1_u^{(4)}$. The upper is for Cl_2, the middle is for Br_2, and the bottom is for I_2.

$$|1\text{st } {}^3\Sigma_u^-\rangle = \cos\theta \cdot |{}^3\Sigma_u^-(1441)\rangle - \sin\theta \cdot |{}^3\Sigma_u^+(2332)\rangle$$
$$|2\text{nd } {}^3\Sigma_u^+\rangle = \sin\theta \cdot |{}^3\Sigma_u^+(1441)\rangle + \cos\theta \cdot |{}^3\Sigma_u^+(2332)\rangle \quad (4)$$

Here, θ is the R-dependent unitary transformation angle. Because such mixed SFCI eigenstates are not useful as the bases to characterize the SOCI wavefunctions, we back-transform the above Eq. (4) to define the "diabatic" bases, $|{}^3\Sigma_u^+(1441)\rangle$ and $|{}^3\Sigma_u^-(2332)\rangle$, and use them as the bases in Eq. (1), along with the three other SF bases. As we will explain later, the second term in Eq. (3) can be negligible in these bases, and the general behavior of the coupling elements can be understood only by the R dependence of the expansion coefficients $\alpha_{i,m}$. In this sense, these five bases play a role of the quasi-diabatic bases.

Figure 3 shows the R dependence of the squared values of $\alpha_{i,m}$ for m = 1, 2, namely for $1_u^{(1)}$ and $1_u^{(2)}$, while Figure 4 shows that for $1_u^{(3)}$ and $1_u^{(4)}$. Another way to see the R dependence of the SOCI wavefunctions is projecting the wavefunctions onto those at the dissociation limits. Such results for $1_u^{(1)}$ and $1_u^{(2)}$ are shown in Figure 5, and those for $1_u^{(3)}$ and $1_u^{(4)}$ in Figure 6. Note that the calculated R_e is 3.811 bohr[25] for Cl_2, 4.340 bohr for Br_2, and 5.099 bohr for I_2.

In Figures 3 and 4, one can easily observe that, in the FC region of Cl_2, each SOCI wavefunction can be represented very well only by the dominant SF component, namely the *LS*-coupling scheme is extremely good, while in the FC region of I_2, strong SO configuration mixings, namely a partial *jj*-coupled behavior can be seen due to the large SO interactions. Looking at the asymptotic regions, for each SOCI wavefunction for $1_u^{(m)}$, the expansion coefficients $\alpha_{i,m}$ show similar behavior and in fact converge to the same limiting values, which are exclusively determined by the angular momentum coupling of the two open-shell halogen atoms, and are therefore independent of the halogen atoms.[19,20] From Figure 3 and also from Figure 5, the electronic wavefunctions for $1_u^{(1)}$ and $1_u^{(2)}$, both converging to the X+X dissociation limits (see Figures 1 and 2) show a noncrossing-type nonadiabatic behavior. Taking into account the slower *LS*-to-*jj* transitions for heavier molecules as seen especially in Figure 5, we can expect more adiabatic behavior, namely smaller magnitude of g_{12} for I_2.

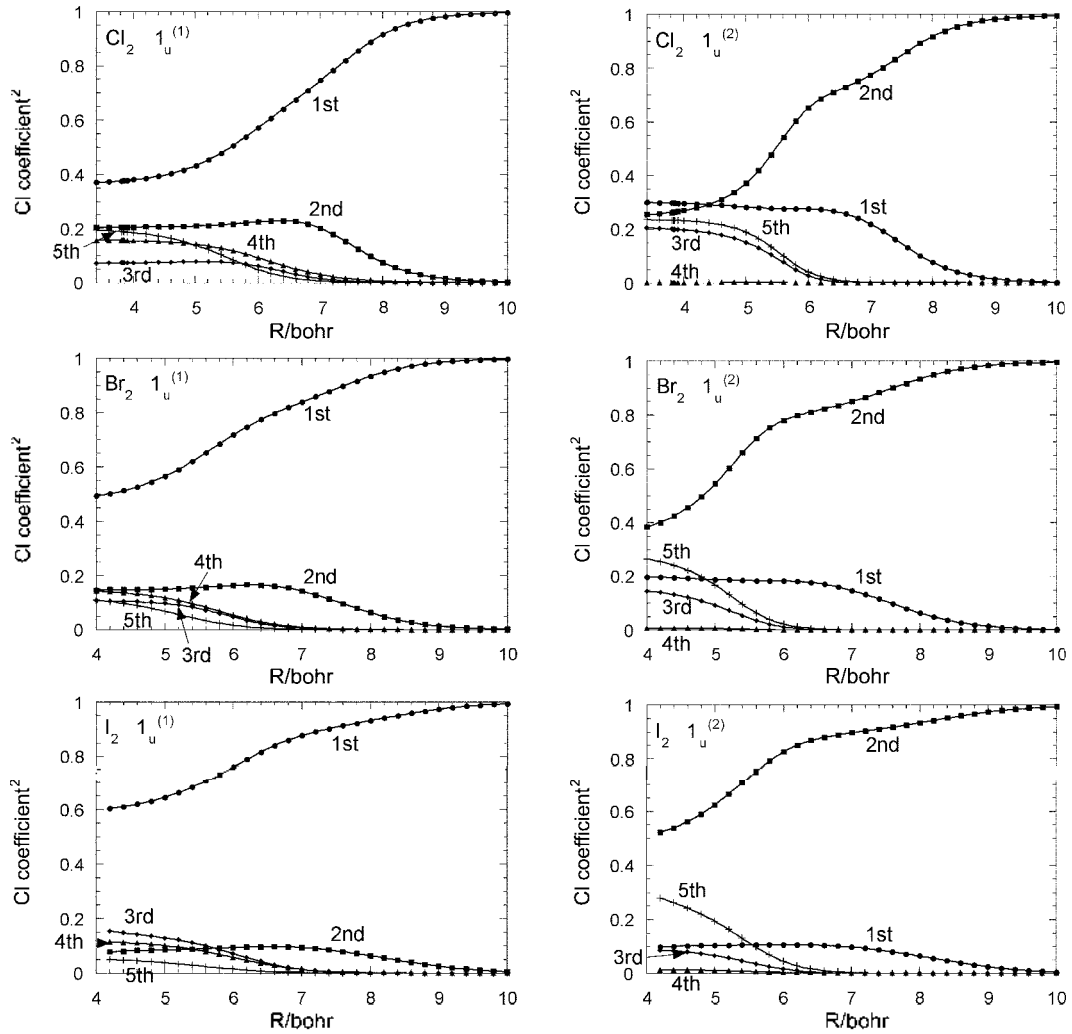

Figure 5. Variations of the weights of the five *jj*-components to expand the adiabatic states $1_u^{(1)}$ and $1_u^{(2)}$. The upper is for Cl_2, the middle is for Br_2, and the bottom is for I_2.

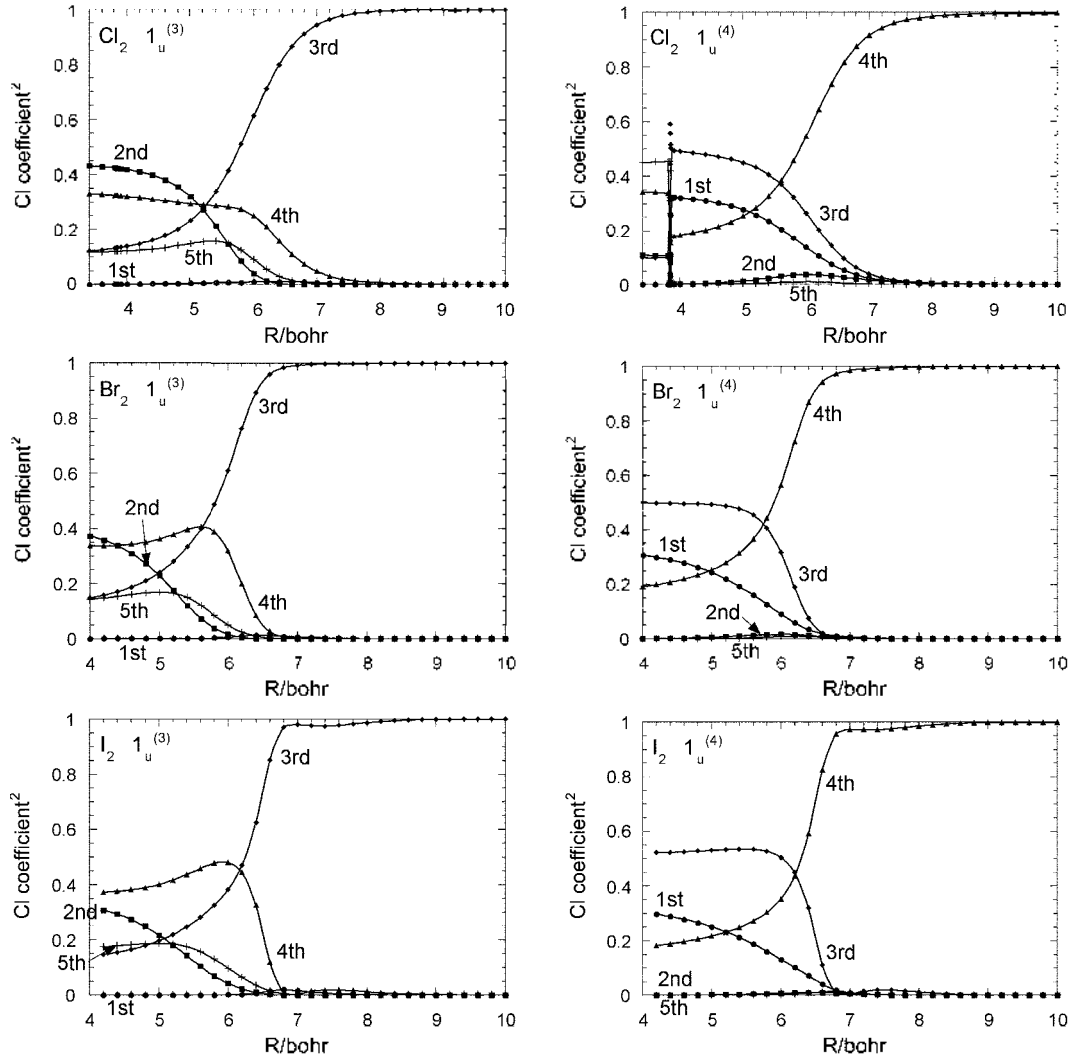

Figure 6. Variations of the weights of the five *jj*-components to expand the adiabatic states $1_u^{(3)}$ and $1_u^{(4)}$. The upper is for Cl_2, the middle is for Br_2, and the bottom is for I_2.

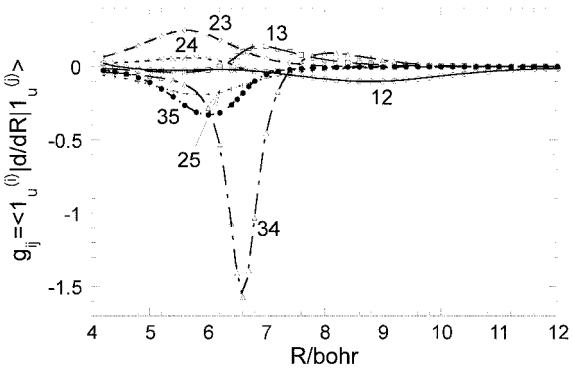

Figure 7. *R* dependence of radial derivative coupling elements g_{ij} for I_2 between states *i* and *j*. Note similarities[5] in Cl_2, Br_2, and I_2.

On the other hand, Figures 4 and 6 show that the SOCI wavefunctions for $1_u^{(3)}$ and $1_u^{(4)}$ exhibit a crossing-type nonadiabatic behavior, and the crossing between $^3\Sigma_u^-$ (1441) and $^3\Sigma_u^+$ (2332) takes place more sharply in the order of Cl_2, Br_2, and I_2, suggesting the increase of the magnitude of g_{34} in this order.

In Figure 4, the electronic wavefunction for $1_u^{(4)}$ of Cl_2 shows a clear crossing behavior between the $^3\Delta_u$ (2332) and $^3\Sigma_u^+$ (2332) configurations at around $R = 3.84$ bohr just outside $R_e = 3.811$ bohr.[2,5] This crossing is very sharp because these two configurations have no direct interaction due to the selection rule of the SO Hamiltonian.[21]

Figure 7 shows the *R* dependence of the radial derivative coupling elements g_{mn} of I_2. They exhibit some similarities to Cl_2 and Br_2.[5,6] As will be seen in Eq. (7) later, these elements are essential for the discussion on the nonadiabatic transitions.

The coupling elements g_{12} and g_{34} between the two states correlating to the same dissociation limits, show the strong dependence on the halogen atoms, as seen from their absolute peak values g_{mn}^{max} shown in the diagonal blocks in Table 3. As suggested before, the g_{12}^{max} value decreases slowly as the molecule changes from Cl_2 through I_2, while the g_{34}^{max} value increases dramatically. The behavior of g_{mn} is largely determined by the balance between the exchange interactions and the SO interactions. The former interactions originate from the Coulombic interactions and represent the

Table 3. Absolute peak values of the radial derivative coupling elements g_{ij}^{max} and their peak distances R_{max}[a]

(a) Between $1_u^{(1)}$ and $1_u^{(2)}$

			Spin-orbit potentials		
Coulombic potentials		SF	Cl_2	Br_2	I_2
Cl_2	g_{12}^{max} (bohr^{-1})	0.0	0.223	0.180	
	R_{max} (bohr)		7.7	7.2	
Br_2	g_{12}^{max} (bohr^{-1})	0.0	0.188	0.160	
	R_{max} (bohr)		8.7	8.0	
I_2	g_{12}^{max} (bohr^{-1})	0.0			0.102
	R_{max} (bohr)				8.8

(b) Between $1_u^{(3)}$ and $1_u^{(4)}$

			Spin-orbit potentials		
Coulombic potentials		SF	Cl_2	Br_2	I_2
Cl_2	g_{34}^{max} (bohr^{-1})	0.316	0.440	1.174	
	R_{max} (bohr)	5.9	6.2	5.7	
Br_2	g_{34}^{max} (bohr^{-1})	0.338	0.347	0.920	
	R_{max} (bohr)	6.4	6.4	6.3	
I_2	g_{34}^{max} (bohr^{-1})	0.328			1.571
	R_{max} (bohr)	7.1			6.6

[a]The diagonal blocks, namely the results obtained by the Coulombic potential and spin-orbit potential for the same atoms, denote the actual values for Cl_2, Br_2, and I_2, and the off-diagonal blocks show the results for the artificial molecules obtained by the combination of the specified Coulombic and spin-orbit potentials.[22,23] The column of SF (spin-free) stands for the results without the spin-orbit interactions.

spatial overlap of the valence atomic orbitals, and the latter ones reflect the heaviness of the halogen atoms.

For examining their dependence on the exchange and SO interactions separately, we calculated g_{12}^{max} and g_{34}^{max} for the artificial molecules by exchanging the SO potentials[22,23] for Cl_2 and Br_2. It should be noted that in the RECP method,[22] the exchange of the SO potentials for the valence electrons can readily be carried out. The results are summarized in the off-diagonal blocks in Tables 3(a) for g_{12}^{max} and 3(b) for g_{34}^{max}, respectively. The use of the same SO potentials and the change of the Coulombic potentials from Cl_2 to Br_2 decreases both g_{12}^{max} and g_{34}^{max}. The magnitude of the exchange interaction, J, between the two atomic orbitals behaves as $J \approx Ae^{-\alpha R}$. Since Br_2 has more diffuse valence orbitals, namely has a smaller α than Cl_2, the exchange interaction for Br_2 decreases more slowly as R increases. In the simple Rosen-Zener-Demkov model, which the nonadiabatic behavior between the states $1_u^{(1)}$ and $1_u^{(2)}$ approximately follows,[5] the peak value is expressed as $g^{max} = \alpha/4$, which is independent of the splitting energy Δ at $R = \infty$ (see Eq. (1) in ref 5). Therefore, the larger atomic orbitals yield smaller peak values, as observed in Tables 3(a) and 3(b).

If we use the same Coulombic potentials but change the SO potentials[22,23] from Cl_2 to Br_2, g_{12}^{max} decreases while g_{34}^{max} increases. As we have discussed before, slower *LS*-to-*jj* transitions for heavier molecules result in smaller g_{12}^{max} values. This is true since the nonadiabatic interaction between $1_u^{(1)}$ and $1_u^{(2)}$ is a non-crossing type.

On the other hand, the nonadiabatic interaction between $1_u^{(3)}$ and $1_u^{(4)}$ is a crossing type, as stated before. We first examine the behavior of g_{34} without the SO interactions. In this case, the corresponding SF adiabatic states are the $|1st\ ^3\Sigma_u^+\rangle$ and $|2nd\ ^3\Sigma_u^+\rangle$ states in Eq. (4), which are expressed in terms of the diabatic bases $^3\Sigma_u^-(1441)$ and $^3\Sigma_u^-(2332)$. Now, by treating the unitary transformation coefficients, $\cos\theta$ and $\sin\theta$, as the expansion coefficients $\alpha_{i,m}$ in Eq. (1), g_{34} in this SF case can be written from Eq. (3) as follows:

$$g_{34}^{SF} = \langle \Psi_3^{SF} \left| \frac{d}{dR} \right| \Psi_4^{SF} \rangle = \frac{d\theta}{dR} + \langle {}^3\Sigma_u^-(1441) \left| \frac{d}{dR} \right| {}^3\Sigma_u^+(2332) \rangle \tag{5}$$

Here, the first term is dominating and the second term has only a negligible contribution (less than 3%), since the latter is the radial derivative coupling element in the diabatic states. Table 3(b) shows that the SF calculations of Cl_2, Br_2, and I_2 yield almost the same g_{34}^{max} values, while R_{max}, where the coupling element has a peak value, increases in the order of Cl_2, Br_2, and I_2, reflecting the size of the valence atomic orbitals.

This Table 3(b) also shows that the inclusion of the SO interactions increases g_{34}^{max} dramatically in this order, while their R_{max} values are about the same. This suggests that the difference in the behavior of g_{34}^{max} comes from the SO interactions, and not from the Coulombic interactions. The wavefunction analyses in Figures 4 and 6 show that the switching of these dominant configurations takes place more sharply in this order around each crossing distance R_{max}. An illuminating point is, as seen in Figure 4, this configuration switching is assisted by the presence of other SF states, such as $^3\Delta_u$ and $^1\Pi_u$, both of which have second order SO interactions with these two $^3\Sigma_u^-$ states. Note also that the first order SO interaction between the diabatic states $^3\Sigma_u^+(1441)$ and $^3\Sigma_u^+(2332)$ is zero due to the selection rule of the SO Hamiltonian.[21] As seen in Figures 4 and 6, these wavefunctions of heavier molecules tend to shift to the *jj*-coupled characters, namely those at the dissociation limits, more quickly around the crossing regions. This is consistent with the dramatic increase in g_{34}^{max} as the magnitude of the SO potentials increases, as shown in Table 3(b).

From these analyses, the g_{12}^{max} value decreases in the order of Cl_2, Br_2, and I_2 because of the additive contributions of the slower variations in the exchange interactions and the slower *LS*-to-*jj* transitions for the heavier systems. As for g_{34}^{max}, however, I_2 has the largest value because it exhibits sharper *LS*-to-*jj* transition at the crossing region, which is not overwhelmed by a relatively smaller contribution of the exchange interactions to reduce g_{34}^{max}.

Numerical estimates of nonadiabatic transition probabilities. In the semiclassical theory, the total wavefunction $\Psi_e(R(t),\mathbf{r})$ satisfies the following time-dependent Schrödinger equation,[19,24]

$$i\hbar \frac{\partial \Psi_e(R(t),\mathbf{r})}{\partial t} = [H_e(R(t),\mathbf{r})]\Psi_e(R(t),\mathbf{r}) \tag{6}$$

where H_e is the electronic Hamiltonian including the SO interactions, **r** is the electronic coordinate, and $R(t)$ is the internuclear distance, and the molecular rotation is not considered in this work. If Ψ_e is expanded in terms of the adiabatic wavefunctions, $1_u^{(1)}$ through $1_u^{(5)}$, the expansion coefficients $C_n(t)$ satisfy a set of the first-order coupled equations.[19,24]

$$i\hbar\frac{dC_k(t)}{dt} = \sum_n [E_k\delta_{kn} - i\hbar v g_{kn}]C_n(t) \tag{7}$$

where E_k are the adiabatic eigenvalues of H_e, namely the SOCI energies, v is the relative nuclear velocity, g_{kn} are the radial derivative coupling elements between $1_u^{(k)}$ and $1_u^{(n)}$ defined in Eq. (2), and $|C_n(t)|^2$ stands for the probability to find the system in the adiabatic state $1_u^{(n)}$. Here, the relative nuclear motion is described by the classical equation of motions.

$$\mu\frac{d^2R(t)}{dt^2} = -\frac{\partial E_i(R)}{\partial R} \tag{8}$$

where μ is the reduced mass and $E_i(R)$ is the adiabatic potential energy on which the photodissociation takes place. Use of the so-called "mean-field potential" $\sum_{i=1}^{5} |C_i(t)|^2 E_i(R)$ instead of $E_i(R)$ in Eq. (8) had negligible effects in the nonadiabatic transition probabilities, typically less than 1%.

General behavior of the state populations for Cl_2 and Br_2 was described before.[6] Figure 8(a) shows the probabilities of I_2 after the vertical excitation to the B" $^1\Pi_u$ ($1_u^{(2)}$) state. Only the nonadiabatic transition from $1_u^{(2)}$ to $1_u^{(1)}$ is observed as in Br_2. This transition probability decreases in the order of Cl_2, Br_2, and I_2. The transition probabilities to the remaining states were negligible, and in the order of 10^{-10} or less. Note that Cl_2 exhibits a small amount of nonadiabatic transition to $1_u^{(3)}$, which can be approximated by the Rosen-Zener-Demkov model[2,5,6] but the corresponding transition does not occur in I_2.

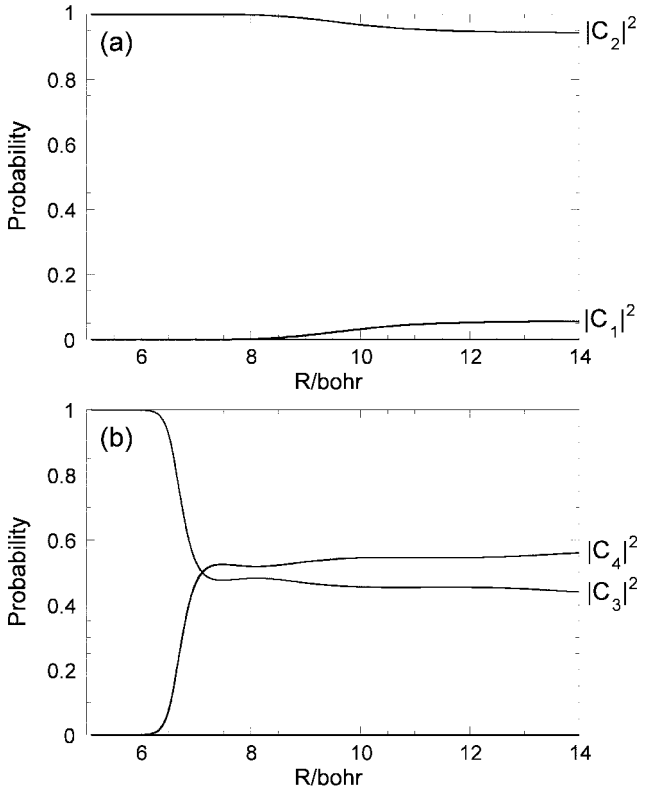

Figure 8. (a) Semiclassical probabilities from the vertical excitation to the B" $^1\Pi_u$ ($1_u^{(2)}$) state of I_2. (b) Similar probabilities from the vertical excitation to the C $^3\Sigma_{1u}^+$ (1441) ($1_u^{(3)}$) state of I_2.

Figure 8(b) shows the probabilities of I_2 after the vertical excitation to the C $^3\Sigma_{1u}^+$ (1441) ($1_u^{(3)}$) state. Only the nonadiabatic transition from $1_u^{(3)}$ to $1_u^{(4)}$ was observed as in Br_2. This transition probability increases in the order of Cl_2, Br_2, and I_2. The transition probabilities to the remaining states were negligible, and in the order of 10^{-9} or less. Note that in the case of Cl_2, the transition to $1_u^{(5)}$ was also found.[6]

The above-mentioned behavior can be understood mostly from the magnitudes as well as the R dependence of g_{mn} and the adiabatic energy difference in the transition regions, the last of which is closely related to the atomic SO splittings. For Cl_2 with a smaller SO splitting, nonadiabatic transitions can occur even between the states correlating to different dissociation limits. For Br_2 and I_2, because of their larger SO splittings, nonadiabatic transitions do not take place between the states correlating to different dissociation limits, but occur only between the states correlating to the same dissociation limits. In the latter case, the magnitudes of g_{mn} determine the nonadiabatic transition probabilities. Since g_{12}^{max} decreases in the order of Cl_2, Br_2, and I_2, the transition probability from $1_u^{(2)}$ to $1_u^{(1)}$ also decreases in this order. On the other hand, the transition probability from $1_u^{(3)}$ to $1_u^{(4)}$ increases in this order, reflecting the dramatic increase of g_{34}^{max}. All these results are consistent with our previous analyses[5,6] and support our interpretation of the nonadiabatic transition mechanism.

For examining the characteristics of these nonadiabatic transitions with higher photon energies, we calculated the transition probabilities at a high energy limit with the initial condition that the molecules dissociate with a very large velocity, $v \sim 1000$ a.u at $R = R_e$. The state populations derived from the vertical excitation to the $^1\Pi_u$ ($1_u^{(2)}$) states and those

Table 4. (a) Semiclassical probabilities derived from the vertical excitation to the $^1\Pi_u$ ($1_u^{(2)}$) states of Cl_2, Br_2, and I_2 at the high energy limit. (b) Similar probabilities derived from the vertical excitation to the $^3\Sigma_{1u}^+$ (1441) ($1_u^{(3)}$) states

(a) From the initial excitation to the $^1\Pi_u$ ($1_u^{(2)}$) state

	$\|C_1\|^2$	$\|C_2\|^2$	$\|C_3\|^2$	$\|C_4\|^2$	$\|C_5\|^2$
Cl_2	0.293	0.271	0.200	6.34×10^{-4}	0.234
Br_2	0.194	0.415	0.141	6.65×10^{-3}	0.243
I_2	0.104	0.644	6.30×10^{-2}	1.05×10^{-2}	0.178

(b) From the initial excitation to the $^3\Sigma_{1u}^+$ (1441) ($1_u^{(3)}$) state

	$\|C_1\|^2$	$\|C_2\|^2$	$\|C_3\|^2$	$\|C_4\|^2$	$\|C_5\|^2$
Cl_2	8.00×10^{-4}	0.418	0.145	0.317	0.119
Br_2	5.15×10^{-4}	0.349	0.158	0.339	0.154
I_2	1.98×10^{-4}	0.200	0.215	0.400	0.186

to the $^3\Sigma_{1u}^-(1441)$ ($1_u^{(3)}$) states are summarized in Tables 4(a) and 4(b), respectively. At this high energy limit, the nonadiabatic transitions can take place between the states correlating to the different dissociation limits even in Br_2 and I_2. However, by calculating the probabilities further with various kinetic energies, it becomes clear that such transitions do not occur at the wavelengths usually used in photochemical experiments, namely $h\nu$ = 10-20 eV.

It is interesting to note that at this high energy limit, namely the diabatic or sudden limit, the final amplitude for each of the atomic state is obtained by projecting the atomic dissociation states on the molecular wavefunction at the FC region.[25] Therefore, the transition probabilities are simply evaluated from the squared overlap between the wavefunctions at $R = R_e$ and those at the dissociation limits, namely those at $R = R_e$ in Figures 5 and 6. Note the calculated R_e is 3.811 bohr[2,5] for Cl_2, 4.340 bohr for Br_2, and 5.099 bohr for I_2. For example, the state populations derived from the vertical excitation to $^1\Pi_u$ ($1_u^{(2)}$) in Table 4(a) coincide with the configuration weights of the electronic wavefunction $1_u^{(2)}$ at $R = R_e$ shown in Figure 5. Those from the vertical excitation to $^3\Sigma_{1u}^-(1441)$ ($1_u^{(3)}$) in Table 4(b) are also in good accord with the configuration weights of $1_u^{(3)}$ at $R = R_e$ shown in Figure 6.

Before concluding the present work, comparison with recent experimental results is in order. As discussed before,[6] our theoretical transition probabilities are in reasonable agreement with recent experiments for both transitions, from $1_u^{(2)}$ to $1_u^{(1)}$ and from $1_u^{(3)}$ to $1_u^{(4)}$, though there is no available experiment for I_2. For the former transition in Cl_2, Brouard *et al.*[4] recently pointed out that the available experimental transition probability[1-4] decreases as the wavelength decreases, that is counterintuitive from a theoretical viewpoint. Our theoretical transition probability shows a very weak wavelength dependence in the opposite and normal direction, e.g. 0.25 at λ = 355 nm and 0.26 at λ = 308 nm. Although this theoretical value at λ = 308 nm is in good agreement with their experimental value of 0.23, careful analyses would be required in both theory and experiment. We suggest more detailed experiments including F_2 and I_2.

Conclusion

We calculated the ground and lower-lying excited states of I_2 by the spin-orbit configuration interaction (SOCI) method, and examined the nonadiabatic dissociation processes that cause the SO branchings of the products, and compared the results to those of Cl_2 and Br_2.

From the configuration analyses, it was found that the nonadiabatic transition between $1_u^{(2)}$ and $1_u^{(1)}$ is a non-crossing type, while that between $1_u^{(3)}$ and $1_u^{(4)}$ is a crossing type for all the three molecules. Variations of the peak values of the radial derivative coupling element between $1_u^{(1)}$ and $1_u^{(2)}$ and that between $1_u^{(3)}$ and $1_u^{(4)}$ can be interpreted by the balance of the Coulombic and SO interactions.

The nonadiabatic transition probabilities were evaluated by the semiclassical theory. In I_2 with the larger SO splitting, the nonadiabatic transitions take place only between the states correlating to the same dissociation limits, as in Br_2. At the high energy limit, the calculated transition probabilities were in good accord with the squared overlap between the wavefunctions at $R = R_e$ and those at the dissociation limits.

For further details, it is necessary to use a more rigorous quantum-mechanical method including the rotational nonadiabatic transitions between asymptotically degenerate states. Such work is now in progress in our laboratory.

Acknowledgment. This work was supported in part by Grants-in-Aids for Scientific Research and for the 21st Century COE program "KEIO LCC" both from the Ministry of Education, Science, Culture, and Sports of Japan.

References

1. Bracker, A. S.; Wouters, E. R.; Suits, A. G.; Vasyutinskii, O. S. *J. Chem. Phys.* **1999**, *110*, 6749.
2. Alexander, A. J.; Kim, Z. H.; Kandel, S. A.; Zare, R. N.; Rakitzis, T. P.; Asano, Y.; Yabushita, S. *J. Chem. Phys.* **2000**, *113*, 9022.
3. Rakitzis, T. P.; Kitsopoulos, T. N. *J. Chem. Phys.* **2002**, *116*, 9228.
4. Bass, M. J.; Brouard, M.; Clark, A. P.; Vallance, C.; Martinez-Haya, B. *Phys. Chem. Chem. Phys.* **2003**, *5*, 856.
5. Asano, Y.; Yabushita, S. *J. Phys. Chem. A* **2001**, *105*, 9873.
6. Asano, Y.; Yabushita, S. *Chem. Phys. Lett.* **2003**, *372*, 348.
7. Li, J.; Balasubramanian, K. *J. Mol. Spectrosc.* **1989**, *138*, 162.
8. Teichteil, C.; Pelissier, M. *Chem. Phys.* **1994**, *180*, 1.
9. de Jong, W. A.; Visscher, L.; Nieuwpoort, W. C. *J. Chem. Phys.* **1997**, *107*, 9046.
10. LaJohn, L. A.; Christiansen, P. A.; Ross, R. B.; Atashroo, T.; Ermler, W. C. *J. Chem. Phys.* **1987**, *87*, 2812.
11. Yabushita, S.; Morokuma, K. *Chem. Phys. Lett.* **1990**, *175*, 518.
12. Amatatsu, Y.; Morokuma, K.; Yabushita, S. *J. Chem. Phys.* **1991**, *94*, 4858.
13. Shepard, R.; Shavitt, I.; Pitzer, R. M.; Comeau, D. C.; Pepper, M.; Lischka, H.; Szalay, P. G.; Ahlrichs, R.; Brown, F. B.; Zhao, J.-G. *Int. J. Quantum. Chem. Symp.* **1988**, *22*, 149.
14. Morokuma, K.; Yamashita, K.; Yabushita, S. *Potential Energy Surfaces of Several Elementary Chemical Reactions*. In *Supercomputer Algorithms for Reactivity, Dynamics and Kinetics of Small Molecules*; Lagana, A., Ed.; Kluwer: Dordrecht, The Netherlands, 1989; p 37.
15. Yabushita, S.; Zhang, Z.; Pitzer, R. M. *J. Phys. Chem. A* **1999**, *103*, 5791.
16. Huber, K. P.; Herzberg, G. *Constants of Diatomic Molecules*; Van Nostrand Reinhold: New York, 1979.
17. Coxon, J. A. In *Low-lying Electronic States of Diatomic Halogen Molecules*; Barrow, R. F.; Long, D. A.; Millen, D. J., Eds.; Molecular Spectroscopy Vol. 1; The Chemical Society: London, 1973; p 177.
18. Galloy, C.; Lorquet, J. C. *J. Chem. Phys.* **1977**, *67*, 4672.
19. Nikitin, E. E.; Umanskii, S. *Theory of Slow Atomic Collisions*; Springer-Verlag: New York, 1984.
20. Singer, S. J.; Freed, K. F.; Band, Y. B. *Adv. Chem. Phys.* **1985**, *61*, 1.
21. Lefebvre-Brion, H.; Field, R. W. *Perturbations in the Spectra of Diatomic Molecules*; Academic: New York, 1986.
22. Pacios, L. F.; Christiansen, P. A. *J. Chem. Phys.* **1985**, *82*, 2664.
23. Hurley, M. M.; Pacios, L. F.; Christiansen, P. A.; Ross, R. B.; Ermler, W. C. *J. Chem. Phys.* **1986**, *84*, 6840.
24. Nikitin, E. E.; Zülicke, L. *Selected Topics of the Theory of Chemical Elementary Processes*; Lecture Notes in Chemistry 8; Springer-Verlag: Berlin, 1978.
25. Singer, S. J.; Freed, K. F.; Band, Y. B. *J. Chem. Phys.* **1983**, *79*, 6060.